ACS APPLIED MATERIALS & INTERFACES

www.acsami.org

Research Article

Label-Free Surface-Enhanced Raman Spectroscopy Biosensor for On-Site Breast Cancer Detection Using Human Tears

Soogeun Kim, Tae Gi Kim, Soo Hyun Lee, Wansun Kim, Ayoung Bang, Sang Woong Moon, Jeongyoon Song, Jae-Ho Shin,* Jae Su Yu,* and Samjin Choi*

Cite This: *ACS Appl. Mater. Interfaces* 2020, 12, 7897−7904

Read Online

ACCESS | Metrics & More | Article Recommendations | Supporting Information

ABSTRACT: Surface-enhanced Raman scattering (SERS) is an ultrasensitive molecular screening technique with greatly enhanced Raman scattering signals from trace amounts of analytes near plasmonic nanostructures. However, research on the development of a sensor that balances signal enhancement, reproducibility, and uniformity has not yet been proposed for practical applications. In this study, we demonstrate the potential of the practical application for detecting or predicting asymptomatic breast cancer from human tears using a portable Raman spectrometer with an identification algorithm based on multivariate statistics. This potentiality was realized through the fabrication of a plasmonic SERS substrate equipped with a well-aligned, gold-decorated, hexagonal-close-packed polystyrene (Au/HCP-PS) nanosphere monolayer that provided femtomole-scale detection, giga-scale enhancement, and <5% relative standard deviation for reliability and reproducibility, regardless of the measuring site. Our results can provide a first step toward developing a noninvasive, real-time screening technology for detecting asymptomatic tumors and preventing tumor recurrence.

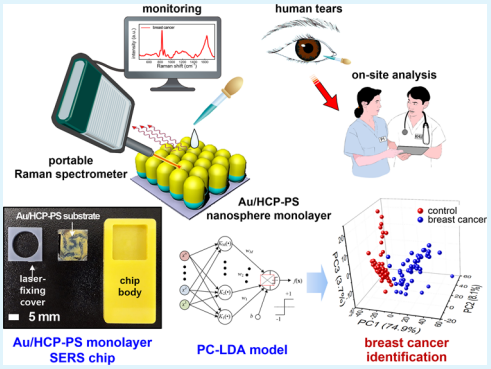

KEYWORDS: *surface-enhanced Raman spectroscopy, breast cancer detection, human tears, Au/HCP-PS nanosphere monolayer, uniformity*

1. INTRODUCTION

Breast cancer is the most common malignant tumor and the main cause of death in women.[1] Approximately one in eight women will be diagnosed with breast cancer during their lifetime. Since 2006, the incidence of breast cancer has increased every year, and is two to six times higher in Asian women. Although the high rate of breast cancer screening has greatly improved the prognosis of breast cancer, the high mortality rate is caused by the delay in early diagnosis. Early detection and appropriate therapy are the most important factors in breast cancer prognosis.[2] Mammography is the best screening test for women over 50 years old, but it has difficulty in detecting small tumors (<1 mm, about 100,000 cells), has inadequate detection of cancer in women with dense breast tissue,[3] and causes breast pain during the mammogram.[4] Serum-based biomarkers, such as carbohydrate antigen 15.3 (CA 15.3) and carcinoembryonic antigen, are used for monitoring ongoing therapy in breast cancer patients with metastatic disease, but there is no biomarker proposed for early detection. Therefore, novel biomarkers or protein profiling in body fluids of breast cancer patients are urgently needed to improve the accuracy of early detection and diagnosis. The research of proteomics and metabolics using body fluids shows the potential of biomarker-based technologies, but there are some problems, such as high cost, time-consuming analytical techniques, and the need for specialists.[5] Recent studies have revealed how rapidly breast cancer can be diagnosed using a label-free method with high sensitivity and specificity.

Tears, which contain mucins, glycoproteins, unglycosylated proteins, peptides, and lipids, are a unique source of body fluids. The major proteins in tears are lysozyme, lactoferrin, secretory immunoglobulin A (sIgA), lipocalin, and lipophilin.[6] The best advantage of tears as a source for a biomarker is that they can be obtained noninvasively, and there is no need to undergo additional protein filtration because they contain few solid proteins, such as albumin. Tears contain around 1500 proteins compared to serum, which contains up to 10,000 proteins.[7] The composition of the tear fluid is changed by variations in response to pathophysiological conditions such as certain ophthalmic or systemic diseases. However, the protein concentration of tears is lower than that of serum and the amount of tears that can be obtained at once from the eyes is very small. Furthermore, diluted tears or eye flush fluids reduce the reliability of protein analysis.[8] Some proteomic studies

Received: October 31, 2019
Accepted: January 23, 2020
Published: January 23, 2020

https://dx.doi.org/10.1021/acsami.9b19421
ACS Appl. Mater. Interfaces 2020, 12, 7897−7904

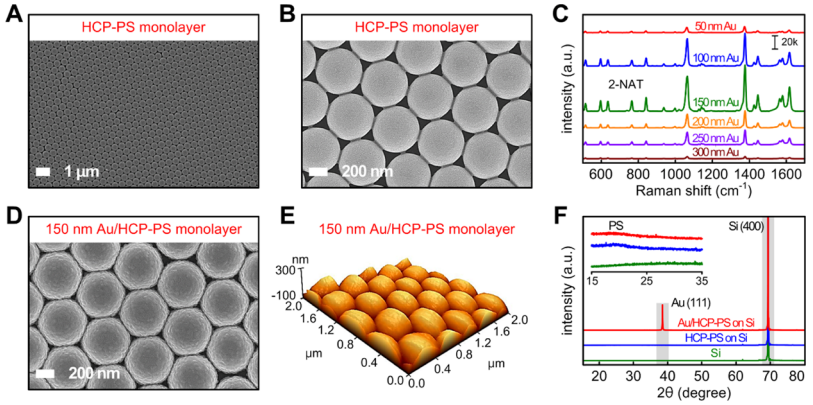

Figure 1. (A,B) FE-SEM images of the HCP-PS monolayer on the Si substrate. (C) Raman spectra at the 785 nm excitation wavelength of 1 mM of the 2-NAT Raman probe molecule on the Au/HCP-PS monolayer with Au thicknesses of 50−300 nm. (D) FE-SEM image and (E) AFM tapping-mode topographical image of the 150 nm thick Au/HCP-PS monolayer. (F) XRD patterns of the Au/HCP-PS monolayer, HCP-PS monolayer, and Si substrate.

reported on potential tear-based biomarkers for breast cancer, such as lacryglobin,[9] eight-biomarker string (3404, 3654, 11,676, 11,742, 16,504, 16,910, 17,503, and 17,542-X),[10] seven-biomarker string (4038, 3629, 92,257, 3785, 3847, 3885, and 3452-X), extracellular sulfatase Sulf-1, cystatin-SA, 5-AMP-activated protein kinase subunit γ-3, and triosephosphate isomerase (>5× decrease).[11] Therefore, a powerful screening technique for the highly sensitive detection and quantification of a variety of specific biofluids is required.

Surface-enhanced Raman scattering (SERS) is a powerful and promising spectroscopic tool for rapid, nondestructive, and ultrasensitive diagnostics.[12] SERS can provide extremely enhanced Raman signals for analytes with small Raman scattering effects at trace levels because of the intense electromagnetic (EM) fields generated by the incident excitation of localized surface plasmon resonance (LSPR) of the plasmonic nanometals.[13] In other words, the well-known hot-spots can be excited when the resonant EM fields are localized at the nanogaps (<10 nm) between adjacent Au nanoparticles and/or near the sharp corners and edges of the metal particles.[14,15] The most important criteria in the practical applications of the substrate-based SERS biosensors are the enhancement factor (EF), reproducibility, and uniformity.[16−18] Metallic SERS substrates with a balance of these criteria will allow for reliable quantitative and qualitative SERS analysis in practice. In previous studies, we analyzed human tears and aqueous humors in various ocular diseases using different SERS substrates.[8,19,20] However, although these SERS substrates showed both high SERS−EF and reproducibility, most SERS substrates showed low uniformity.

In this study, we present a novel strategy and progress in the highly sensitive detection and quantification of tear fluids, and their potential application for breast cancer identification. A SERS substrate was fabricated based on two main stages: the formation of a free-standing monolayer with hexagonal-close-packed (HCP) polystyrene (PS) nanospheres by spin-coating, and then the deposition of an Au layer on the HCP-PS monolayer by e-beam evaporation to complete the plasmonic Au/HCP-PS monolayer. The physical properties of the Au/HCP-PS monolayer were characterized with a field-emission scanning electron microscope, an atomic force microscope, and an X-ray diffractometer. A three-dimensional finite-difference time-domain (3D FDTD) approximation model and trace amounts of a small 2-naphthalenethiol (2-NAT) Raman probe molecule were used to evaluate the SERS performance of the plasmonic Au/HCP-PS monolayer substrate for criteria such as wavelength, $|E|^4$-approximation, signal-to-noise ratio (SNR), sensitivity, limit of detection (LOD), SERS−EF at analytical chemistry conditions, reproducibility, and repeatability. Finally, we demonstrate the great potential in practical applications through the detection or prediction of the asymptomatic breast cancer from human tear fluids using a portable Raman spectrometer device with a multivariate statistics-based identification method.

2. RESULTS AND DISCUSSION

2.1. Fabrication of SERS-Optimized Au/HCP-PS Monolayer. Figure 1A,B shows the field-emission scanning electron microscopy (FE-SEM) images of the HCP-PS monolayer formed on the Si substrate using spin-coating. The HCP-PS nanosphere arrays were formed over a large area (1.5×1.5 cm^2) without any significant voids when spin-coated at a slow speed from a solution with a low volume fraction of ethanol. Multistacked structures were formed when the PS was spin-coated with a large volume fraction of ethanol and at a high spin speed. The very regularly arranged nanostructures were expected to exhibit promising potential in the LSPR effect. The enhancement of Raman intensities was investigated using a 1 mM 2-NAT molecule with a 785 nm excitation wavelength for six Au/HCP-PS nanospheres (Figures 1C and S1). The characteristic peaks of 2-NAT were clearly observed in all the conditions.[21−23] The 150 nm Au/HCP-PS monolayer had the highest SERS activity. This was attributed to the modest nanogap metallic structure that had deep and sharp crevices (Figure 1D,E), forming the so-called hot-spot region. In other words, this excellent SERS performance is likely due to the formation of sub-10 nm gaps (hot-spots) between the Au-coated PS nanospheres, maximizing the LSPR effect. However, further Au-coating led to degradation in Raman intensities. This was caused by the decrease in the number of hot-spots related to wide nanogaps (<150 nm) and/or the presence of shallow and smooth crevices (>150 nm). The gold layer was deposited on half of the PS nanospheres by e-beam evaporation, which had unique characteristics such as directional flow and poor step coverage. The actual Au thickness deposited on the HCP-PS monolayer, as estimated from FE-SEM images, was 67, 126, 172, 223, 239, and 304 nm for the Au thicknesses of 50, 100, 150, 200, 250, and 300 nm,

https://dx.doi.org/10.1021/acsami.9b19421
ACS Appl. Mater. Interfaces 2020, 12, 7897−7904

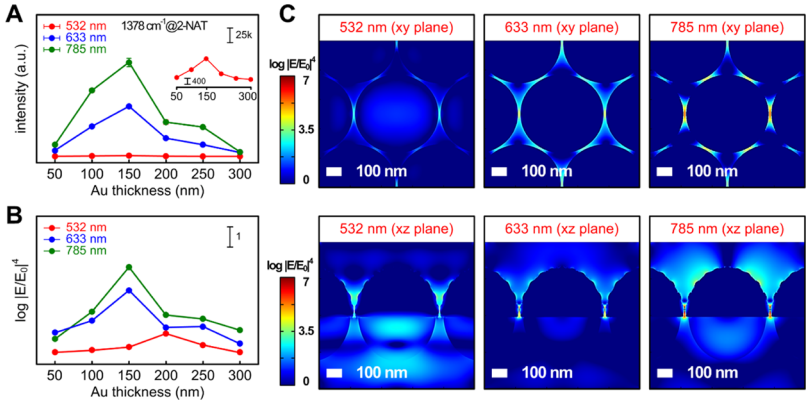

Figure 2. (A) Experimental results—Raman intensities at 1378 cm^{-1} peak of 1 mM of the 2-NAT probe molecule on the Au/HCP-PS monolayer. (B) Computational results——$|E|^4$-approximation of the surface enhanced Raman scattering (SERS) EF of 3D FDTD Au/HCP-PS nanosphere models with Au thicknesses of 50−300 nm at excitation wavelengths of 532, 633, and 785 nm. (C) 3D FDTD computational results of a 150 nm Au/HCP-PS nanosphere model with the highest SERS activity regardless of excitation wavelength.

respectively. A 150 nm Au/HCP-PS monolayer showed the highest atomic force microscopy (AFM)-estimated root-mean-square roughness, caused by the isolated and very narrow hot-spot formation (Figures 1E, S2 and S3). The X-ray diffractometry (XRD) patterns of the Si, HCP-PS/Si, and Au/HCP-PS/Si composites were measured at each process step (Figure 1F). The prominent peaks at the 2θ angles of 38.3 and 69.2° corresponded to the reflections of the Au(111) and Si(400) crystal planes, respectively. The broad reflection at 2θ = 15−25° was assigned to amorphous PS.[24] This confirms that the 150 nm Au/HCP-PS monolayer is successfully fabricated and this nanostructure is likely to provide excellent and stable SERS performance for further applications.

2.2. Wavelength Characteristics of the Au/HCP-PS Monolayer. The effect of wavelength on the SERS performance of the optimized Au/HCP-PS monolayer was investigated experimentally and computationally with three representative Raman excitation wavelength sources, 532, 633, and 785 nm, using 1 mM of 2-NAT. The Raman intensities of 2-NAT increased significantly with increasing wavelength (Figure 2A). The increase was related to the reflection properties of the nanostructure-arrayed surface. The reflection from the surface of a nanostructure array increases sharply with increasing wavelength (λ) when the optical depth (d_{opt}) < 0.4λ.[25] Herein, d_{opt} is defined by

$$d_{opt} = n \cdot d \quad (1)$$

where n and d are the refractive index and coating thickness of Au, respectively. In this study, the optical depth of the thickest Au/HCP-PS monolayer (300 nm thick) was d_{opt} = 164.2 nm (n = 0.54 at 532 nm wavelength and d = 304 nm), which was smaller than 0.4λ = 212.8 nm at the 532 nm excitation wavelength (Table S1). Therefore, the reflection from the Au/HCP-PS monolayer surface increased sharply with increasing wavelength. The 2-NAT Raman intensities increased until the Au thickness equaled 150 nm, which was consistent with the preliminary study.[26] As the Au thickness increased beyond 150 nm, the Raman intensities decreased greatly and were restored to near those of the monolayers with 50 nm thick gold. Similar behavior was observed at all wavelengths. This was related to isolated and very narrow hot-spot regions formed when the Au thickness was near 150 nm, as mentioned above. It also indicated that the hot-spot-generated SERS effect was independent of Raman excitation wavelength sources. Interestingly, the characteristic peaks of 2-NAT excited at the 532 nm wavelength were clearly observed at all Au thickness conditions, even though the SERS signals were very small and contained some noise (Figure S4).

Next, the effect of Au thickness and excitation wavelength on the distribution of the EM field near the surface of the Au/HCP-PS monolayer was investigated with the 3D FDTD method (Lumerical FDTD Solution, version 8.21.1906, Canada). The Au/HCP-PS nanosphere systems were modeled by controlling the nanogaps or crevices, measured from FE-SEM images, between the Au-covered PS nanospheres for each Au thickness (Figure S5). The SERS-EF approximated from the EM mechanism of SERS is generally defined as $|E/E_0|^4$, where E is the local maximum electric field and E_0 is the amplitude of the input source electric field in a linear simulation. The simulated SERS−EF ($|E|^4$-approximation) showed a similar pattern to the Raman intensities of the Au/HCP-PS monolayer (Figure 2B). The distribution of the EM field increased with increasing Au thickness regardless of the wavelength. Also, the presence of a strong EM field in the nanogaps was observed when the Au thickness was 150 nm (Figure 2C and Table S2). Furthermore, the 785 nm excitation wavelength produced a very strong EM field distribution compared to the EM field generated by the 532 nm excitation wavelength. When the Au thickness was greater than 150 nm, the EM field decreased significantly and was restored to near that of when the Au thickness was 50 nm. Because the Raman intensity is inversely proportional to the fourth power of the excitation wavelength, a shorter wavelength source (532 nm) with stronger Raman scattering and better SNR seems to be the best laser source for SERS applications compared to a near infrared wavelength source (785 nm). However, the 532 nm excitation wavelength can cause sample fluorescence in complex organic molecules, whereas the use of a 785 nm excitation wavelength can eliminate sample fluorescence from most organic molecules. We also found that a superior SERS effect was observed with the 785 nm laser source compared to the 532 nm laser source. Therefore, this result suggests that the 785 nm excitation wavelength laser source is suitable for SERS applications of the Au/HCP-PS monolayer SERS substrate.

2.3. SERS Performance of Au/HCP-PS Monolayer. The SERS activity of the 150 nm Au/HCP-PS monolayer was evaluated by analyzing Raman intensities for concentrations of 2-NAT in the range of 10^{-8} to 10^{-3} M (Figure 3A) and 10^{-13}

https://dx.doi.org/10.1021/acsami.9b19421
ACS Appl. Mater. Interfaces 2020, 12, 7897−7904

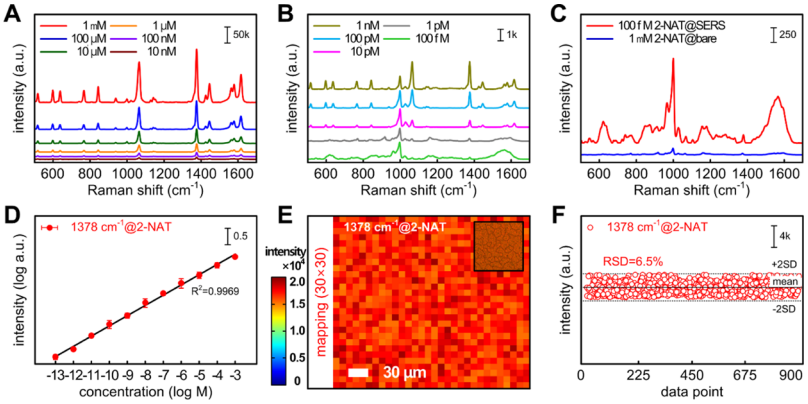

Figure 3. (A,B) Raman spectra with different concentrations of 2-NAT on the optimized Au/HCP-PS monolayer substrate. (C) Raman spectra of 100 fM 2-NAT on an Au/HCP-PS monolayer and 1 mM 2-NAT on a bare HCP-PS monolayer. (D) Linear correlation curve of Raman intensities at 1378 cm^{-1} with the different concentrations of 2-NAT on the plasmonic Au/HCP-PS monolayer (R^2 = 0.9969). (E) Raman mapping and real optic (inset) images of 1 μM 2-NAT with a square of 300 × 300 μm^2 through a 10 μm pitch on the Au/HCP-PS monolayer SERS substrate. (F) High reproducibility with RSD = 6.5% at the 1378 cm^{-1} peak.

to 10^{-9} M (Figure 3B). We could observe the characteristic peaks of 2-NAT, such as 764 cm^{-1} (ring deformation), 1068 cm^{-1} (C−H bending), and 1378 cm^{-1} (ring stretching), even at concentrations as low as 10^{-13} to 10^{-12} M (Figure 3B). Among them, the 1378 cm^{-1} peak with a very strong and clear Raman intensity was used as a representative analysis peak. At first, the LOD, one of the key parameters for evaluating the performance of a SERS biosensor, was investigated. The SNR of the 1378 cm^{-1} peak was calculated to be ~6, using the following formula[27]

$$\mathrm{SNR} = \frac{I}{\sigma_I} \tag{2}$$

where I and σ_I are the average Raman intensity and its standard deviation (based on 10 measurements), respectively. I and σ_I were 120.1 and 20.1, respectively, for the 1378 cm^{-1} peak with a 100 fM 2-NAT concentration. Hence, the LOD of the Au/HCP-PS monolayer was determined to be 100 fM. In order to quantify the SERS-EF of the Au/HCP-PS monolayer substrate, the SERS−EF was calculated using the following formula[28]

$$\mathrm{EF} = \left(\frac{I_{\mathrm{SERS}}}{I_{\mathrm{bare}}}\right)\left(\frac{N_{\mathrm{bare}}}{N_{\mathrm{SERS}}}\right) \tag{3}$$

where I_{SERS} and I_{bare} are the Raman intensities of 2-NAT on the Au/HCP-PS monolayer and on a bare HCP-PS monolayer, respectively. N_{SERS} and N_{bare} are the average number of 2-NAT molecules contributing to the SERS signal and bare Raman signal, respectively. Assuming that 2-NAT is almost uniformly distributed on each monolayer, the average number (N) of 2-NAT molecules contributing to the SERS signal can be estimated as follows

$$N = N_A \cdot c \cdot \frac{V_{\mathrm{droplet}}}{A_{\mathrm{spot}}} \cdot A_{\mathrm{laser}} \tag{4}$$

where N_A is Avogadro's constant, c is the concentration of 2-NAT, $V_{droplet}$ is the volume of the 2-NAT droplet, A_{spot} is the area of the spot formed by the 2-NAT droplet, and A_{laser} is the area of the laser spot. From an analytical chemistry point of view,[29] because the same measurement method and sample preparation conditions were applied to each monolayer substrate, N_A, $V_{droplet}$, A_{spot}, and A_{laser} were the same. Hence, the average number of 2-NAT molecules contributing to the SERS signal (N_{SERS}) and bare Raman signal (N_{bare}) could be replaced with the concentration of 2-NAT on the Au/HCP-PS monolayer (c_{SERS}) and bare HCP-PS monolayer (c_{bare}), respectively. Equation 3 can be written as follows

$$\mathrm{EF} = \left(\frac{I_{\mathrm{SERS}}}{I_{\mathrm{bare}}}\right)\left(\frac{c_{\mathrm{bare}}}{c_{\mathrm{SERS}}}\right) \tag{5}$$

Finally, the SERS−EF of the Au/HCP-PS monolayer was determined to be 5.4 × 10^{10}, where I_{SERS} = 120.1 (c_{SERS} = 100 fM) and I_{bare} = 22.1 (c_{bare} = 1 mM), respectively (Figure 3C). This confirms that the plasmonic Au/HCP-PS monolayer substrate provides precise and sensitive SERS performance in trace detection of biochemicals.

We also investigated the correlation between Raman intensity and c_{SERS}. The Raman intensity decreased monotonically with decreasing c_{SERS} (Figure 3A,B), and the Raman spectral profiles were almost the same until c_{SERS} = 10 pM. Although there were a few distortions of the Raman spectral profile at the 1 pM and 100 fM concentrations, the 2-NAT characteristic Raman peaks at 1068 and 1378 cm^{-1} were clearly observed. This led to an extremely linear correlation curve in the log/log scale (Figure 3D) with log I_{SERS} = 6.2 + 0.3 log(c_{SERS}) (R^2 = 0.9969).

The reliability of the Au/HCP-PS monolayer SERS substrate was evaluated in terms of its reproducibility and repeatability. Raman spectral mapping was conducted with a 300 × 300 μm^2 square through a 10 μm pitch (A_{spot} < 2.4 μm) using 1 μM of 2-NAT (Figure 3E). The Raman mapping image reconstructed from the 900 SERS spectra indicated that the Au/HCP-PS SERS substrate had a uniform ultrastructure with a high reproducibility relative standard deviation (RSD) of 6.5% (Figure 3F, 16,758 ± 1082). Furthermore, the repeatability RSD obtained from 200 repeated measurements at the same measurement point indicated that the Au/HCP-PS SERS substrate had a very high repeatability RSD of 3.5% (Figure S6, 15,758 ± 556). Therefore, these results suggest that the Au/HCP-PS monolayer SERS substrate provides a highly precise, quantitative, and reliable method to be applied to label-free SERS-functionalized biomedical applications based on trace analysis.

https://dx.doi.org/10.1021/acsami.9b19421
ACS Appl. Mater. Interfaces 2020, 12, 7897−7904

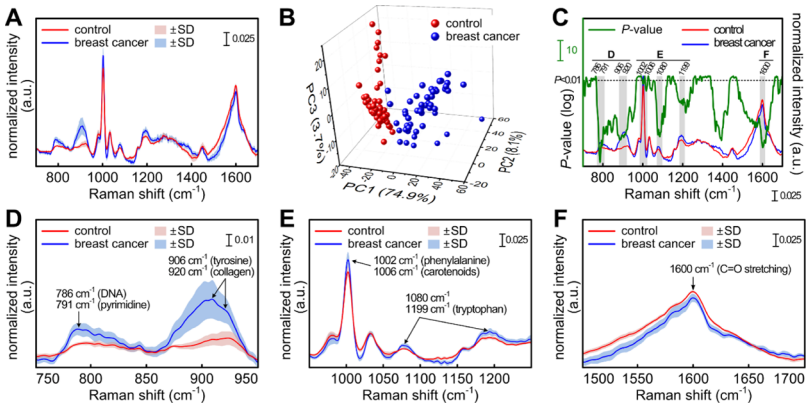

Figure 4. Bioapplication of a portable Raman spectrometer device with a multivariate statistics-based identification method to detect the presence of asymptomatic breast cancer using human tear fluids. (A) Preprocessed SERS spectra of tear fluids for five healthy controls and five patients with breast cancer. (B) Cluster plot of principal component analysis (PCA) scores for 100 Raman spectra of five healthy controls (50 spectra) and five patients (50 spectra) with breast cancer, with percentage of variances for PC1 = 74.9%, PC2 = 8.1%, and PC3 = 3.7%. (C) Student's two-sided *t*-test on Raman peak intensities of the two groups over the entire spectral range (700−1700 cm^{-1}). Local Raman spectra in (D) 750−950, (E) 950−1250, and (F) 1500−1700 cm^{-1}.

2.4. Analysis of Breast Cancer Using Tear Fluids. The feasibility and versatility of the plasmonic Au/HCP-PS monolayer substrate as a biosensor (Figure S7) were evaluated by analyzing for breast cancer using human tear fluids. Figure 4A shows the preprocessed SERS spectra of two tear fluid groups obtained from five healthy controls and five patients with breast cancer using a portable Raman spectrometer device. Each heavy line represents the average SERS signals calculated from 50 Raman spectra per group. Vector normalization based on the Euclidean norm[30] was performed to eliminate disparities in intensity levels caused by the different concentrations of each tear fluid sample and not related to the intrinsic differences between the groups. Overall, both groups showed the following distinctive Raman peaks:[31−34] O−P−O stretching and cytosine, uracil, and thymine in DNA at 786 cm^{-1}, pyrimidine at 791 cm^{-1}, tyrosine at 906 cm^{-1}, collagen at 920 cm^{-1}, phenylalanine at 1002 cm^{-1}, carotenoids at 1006 cm^{-1}, tryptophan at 1080 cm^{-1}, tryptophan ring breathing at 1199 cm^{-1}, and C═O stretching at 1600 cm^{-1}. Because the two groups showed different SERS profiles for these Raman peaks, they were likely to be used as a biomarker for identifying the presence of breast cancer.

The principal component linear discriminant analysis (PC-LDA) identification method with small sample sizes was implemented with the Au/HCP-PS monolayer SERS sensor to identify the breast cancer from human tear fluids. The global spectral features of each group were extracted and all SERS spectral peaks were used for the PCA computation. The cluster plot of loading profiles on the PCs for the healthy control group and the breast cancer group (Figure 4B) indicated that our PC-LDA identification method was useful to discriminate between the two groups. The PC variance used for this identification totaled 86.7% for total spectral variations, with 74.9% for PC1, 8.1% for PC2, and 3.7% for PC3. The corresponding PC loading data included the Raman peaks that play an important role in the identification of breast cancer (Figure S8), such as 906, 920, 1002, 1006, and 1600^{-1}. Interestingly, these Raman peaks in the PC loading profiles were consistent with the distinctive Raman peaks (biomarker) observed in the raw Raman spectra both groups (Figure 4A). This indicated that the result extracted from the PCA algorithm result reflected well the Raman peak intensity information between the two groups. The leave-one-out cross-validation (LOOCV)-assisted PC-LDA identification method provided the confusion matrix with classification accuracy of 96% (Table 1). It achieved a clinical sensitivity of 92% and a specificity of 100% for tear-fluid-based asymptomatic breast cancer identification. In addition, Student's two-tailed *t*-test between the two groups was performed in order to verify the biomarkers (Raman peaks) used in the PC-LDA identification method (Figure 4C). Overall, the calculated *P*-values were very small (less than 10^{-19}) for the proposed biomarkers, except for the 1002 and 1006 cm^{-1} peaks. This identification method could be used to identify or predict the presence of breast cancer using human tear fluids.

Table 1. PC-LDA-Analyzed Confusion Matrix for Tear Fluid-Based Breast Cancer Identification[a]

		actual	
		breast cancer	control
predicted	breast cancer	46 (TP)	0 (FP)
	control	4 (FN)	50 (TN)

[a]TP, true positive. FP, false positive. FN, false negative. TN, true negative.

Verification of the relationship between the proposed biomarker and breast cancer is very important in interpreting tear-fluid-based breast cancer identification. At first, Leon et al.[35] reported an increase in serum levels of cell-free nucleic acid in patients with breast cancer. Silva et al.[36,37] also detected genetically altered and methylated cell-free nucleic acid in the plasma of patients with breast cancer. An increase of cell-free nucleic acid in the blood of breast cancer patients is related to excessive DNA release by apoptotic and necrotic cells during tumor development.[38] This increase is consistent with our results that the DNA-assigned 786 cm^{-1} Raman peaks of the breast cancer patients were 4.03 times higher than those of the healthy controls (Figure 4D). In addition, impaired organ function during systemic inflammation may contribute to cell-free nucleic acid elevation in patients with breast cancer.[39] Tyrosine, phenylalanine, and tryptophan are aromatic amino acids, and phenylalanine and tryptophan are essential amino

https://dx.doi.org/10.1021/acsami.9b19421
ACS Appl. Mater. Interfaces 2020, 12, 7897−7904

Scheme 1. Fabrication Procedure for the Au/HCP-PS Monolayer SERS Substrate

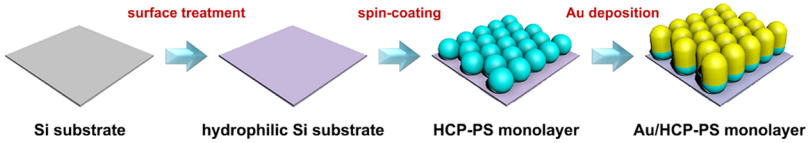

acids in the human diet. Tryptophan metabolism (1080 and 1199 cm^{-1}) is linked to the production of serotonin, and phenylalanine (1002 cm^{-1}) is required for the production of the nonessential amino acid tyrosine (906 cm^{-1}) catalyzed by the enzyme phenylalanine hydroxylase. There seems to be a clear effect of breast cancer on metabolic variables. It has been shown that phenylalanine hydroxylase activity can be altered in malignancy.[40] Hence, the Raman intensities of tyrosine, phenylalanine, and tryptophan in patients with breast cancer may be changed, compared to those of healthy individuals. Poschke et al.[41] reported that breast cancer shows a tumor-dependent increase in serum tyrosine and phenylalanine levels. In particular, phenylalanine is statistically significant in patients with breast cancer. Cascino et al.[42] observed significant increases in free tryptophan through 33 breast cancer patients. Fröbe et al.[43] showed that plasma-free serotonin can be used as a marker of recurrence of breast cancer. They concluded that the changes in tryptophan metabolism in the malignant progression of breast cancer are associated with increased serotonin synthesis. These molecular increases are consistent with our results that some Raman peaks for the breast cancer patients increased compared to the healthy controls, such as 1.18 × (1002 cm^{-1}) for phenylalanine and 5.65 × (1080 cm^{-1}) and 1.43 × (1199 cm^{-1}) for tryptophan (Figure 4D,E). Therefore, it is very important to evaluate the changes in amino acid metabolism to distinguish patients with breast cancer from healthy individuals. Furthermore, the collagen-assigned Raman peak (920 cm^{-1}) can be interpreted by cancer angiogenesis. Mazouni[44] revealed that the levels of plasma collagen IV are significantly higher in patients with breast cancer than in healthy women. Our results also showed that the collagen-assigned Raman intensities of the breast cancer patients were increased 3.66× compared to the healthy controls. Hence collagen IV, which is a major component of the vascular basement membrane, can be considered as a biomarker of angiogenic activity. Lastly, carotenoids (1006 cm^{-1}) are organic pigments that are generally known to have a cancer-protective effect.[45−47] However, the role of carotenoids in breast cancer has not yet been elucidated, and some studies have shown that there is no significant effect on breast cancer prevention.[48] Further studies on the role of carotenoids in patients with breast cancer are needed. It is recognized that the proposed biomarkers are useful to detect asymptomatic breast cancer from human tear fluids using our platform.

3. CONCLUSIONS

In summary, the highly discriminatory power of a portable Raman spectrometer device with a well-aligned Au/HCP-PS monolayer SERS biosensor supported by a multivariate statistics-based identification method indicated that it might be possible to detect or predict asymptomatic breast cancer from human tear fluids. Using a facile spin-coating method, a self-assembled HCP-PS monolayer was constructed without significant voids and multistacked structures (the perfect periodicity), thus exhibiting superior uniformity. The optimized Au thickness was determined to be 150 nm, resulting in the formation of an isolated and very narrow hot-spot showing a giga-scale enhancement and a single-digit reliability. The proposed spectral markers might be directly associated with molecules related to breast cancer. Hence, if appropriate sensitivity is guaranteed, it is anticipated to be the new diagnostic method that can solve the disadvantages of conventional labeling methods such as high expensive and low yield. These results indicate that our noninvasive real-time label-free screening technology can be used immediately for the early detection of asymptomatic tumors, thereby decreasing the likelihood of tumor recurrence (Figure S9).

4. METHODS

4.1. Human Study. Human tears were collected from five healthy control patients (41.2 ± 8.1 yr) and five patients with breast cancer (47.6 ± 7.6 yr) in the Kyung Hee University Hospital in Gangdong. The inclusion criteria of the breast cancer group are presented as follows: female sex, age between 20 and 80 years, who were currently diagnosed with breast cancer. We excluded patients who had difficulty in generating tear components because of inflammation or infection in the anterior segment. Informed consent was obtained from each subject in the Kyung Hee University Hospital at Gangdong. All procedures involving humans adhered to the Declaration of Helsinki and were approved by the Ethical Committee of Kyung Hee University Hospital at Gangdong (KHNMC 2017-08-015).

4.2. Fabrication of the Au/HCP-PS Monolayer. To fabricate the Au/HCP-PS monolayer SERS substrate (Scheme 1), the Si wafer was cut into pieces with a size of 1.5 × 1.5 cm^2. The substrates were cleaned in acetone, methanol, and distilled water successively for 5 min. A piranha solution was also used to eliminate residual impurities. For a hydrophilic surface, the as-prepared Si substrates were treated with a solution containing NH_4OH (Duksan Pure Chemicals, Korea), H_2O_2, and distilled water with a volume ratio of 1:1:5. A solution of PS spheres (Sigma-Aldrich, USA) with average diameter of 500 nm was mixed with ethanol to adjust its volatility. To construct the HCP-PS monolayer, the PS solution was dropped on the Si substrates and spin-coated at 1100 rpm for 20 s. To fabricate the SERS-functionalized substrate, an Au layer was deposited with a KVE-E2004 e-beam evaporator (Korea Vacuum Tech., LTD., Korea) with a deposition rate of 1 Å/s at a voltage <7 kV and a base pressure <3 μTorr at room temperature.

4.3. Preparation of Human Tears. Tears were collected using 10 μL glass microcapillary tubes (Marienfeld Superior, Germany). The capillary tube rested in the lateral tear meniscus. In order to prevent reflex tearing by eye irritation, the contact with the bulbar conjunctiva was minimized. When the microcapillary tube filled to about 1/4 of its entire length, the tears were transferred to a 1.5 mL Eppendorf tube (Eppendorf-Netheler-Hinz GmbH, Germany) using an air syringe. The collection procedure was repeated until collection volumes reached at least 5 μL. All the samples were stored at −80 °C until further processing.

4.4. Characterization. The structural and morphological properties of the Au/HCP-PS monolayer were characterized using an FE-SEM (Hitachi, Japan) with an accelerating voltage of 10 kV and an XE100 AFM (Park Systems Corp., Korea). The crystalline phase of the Au/HCP-PS monolayer was characterized using an M18XHF-SRA XRD (Mac Science, Japan) with Cu Kα (λ = 1.5406 Å) radiation in the 2θ range of 15−80° with a step of 0.02°.

https://dx.doi.org/10.1021/acsami.9b19421
ACS Appl. Mater. Interfaces 2020, 12, 7897−7904

4.5. SERS Measurement. 2-NAT (Sigma-Aldrich) was used as the Raman probe molecule to suppress the coffee ring effect. Raman spectra of 2-NAT on the Au/HCP-PS monolayer SERS chip were obtained using a SENTERRA confocal Raman spectroscope (Bruker Optics, USA) with a 785 nm diode laser with 10 mW of power and a 20× objective lens. Samples were processed within a fingerprint range of 417−1782 cm^{-1} with a spectral resolution of 5 cm^{-1} and twice the acquisition time of 10 s. Measurements were taken at 10 random points using a 2 μL drop of the Raman probe and dried at room temperature. Also, SERS spectra of tear fluids taken from patients with breast cancer in a clinical setting were measured by a handheld Raman spectrometer Mira DS (Metrohm Ag, Switzerland) with the Au/HCP-PS monolayer SERS chip. All the SERS data were analyzed through the PC-LDA identification method, which combined both the PCA and LDA methods. The PC-LDA model was performed with a data-processing procedure consisting of three steps, including smoothing by a Savitzky−Golay filter, baseline-correction by a concave rubber band method, and normalization by a vector normalization technique where each of the Raman intensities corresponding to a Raman shift was divided by the Euclidean norm. To check for overfitting and evaluate the performance of the PC-LDA model on the Au/HCP-PS monolayer SERS chip, a LOOCV was carried out. All the data analyses were performed with R statistical software (Foundation for Statistical Computing, Austria).

■ ASSOCIATED CONTENT

Supporting Information

The Supporting Information is available free of charge at https://pubs.acs.org/doi/10.1021/acsami.9b19421.

FE-SEM images, AFM topographical images, wavelength characteristics, 3D FDTD models, SERS-EF calculation, and repeatability of Au/HCP-PS monolayer on Si substrate; plasmonic Au/HCP-PS monolayer biosensor chip; PC loading profiles of the PCA model for discrimination between healthy control and breast cancer; and practical application (PDF)

■ AUTHOR INFORMATION

Corresponding Authors

Jae-Ho Shin − *Department of Ophthalmology, College of Medicine, Kyung Hee University, Seoul 02447, South Korea*; Email: pbloadsky@naver.com

Jae Su Yu − *Department of Electronic Engineering, Institute for Wearable Convergence Electronics, Kyung Hee University, Gyeonggi-do 17104, South Korea*; orcid.org/0000-0003-0258-7936; Email: jsyu@khu.ac.kr

Samjin Choi − *Department of Biomedical Engineering, College of Medicine, Kyung Hee University, Seoul 02447, South Korea*; orcid.org/0000-0003-3498-0652; Phone: +82 2 961 0290; Email: medchoi@khu.ac.kr; Fax: +82 2 961 5515

Authors

Soogeun Kim − *Department of Biomedical Engineering, College of Medicine, Kyung Hee University, Seoul 02447, South Korea*; orcid.org/0000-0001-5483-6661

Tae Gi Kim − *Department of Ophthalmology, College of Medicine, Kyung Hee University, Seoul 02447, South Korea*

Soo Hyun Lee − *Department of Electronic Engineering, Institute for Wearable Convergence Electronics, Kyung Hee University, Gyeonggi-do 17104, South Korea*

Wansun Kim − *Department of Biomedical Engineering, College of Medicine, Kyung Hee University, Seoul 02447, South Korea*

Ayoung Bang − *Department of Biomedical Engineering, College of Medicine, Kyung Hee University, Seoul 02447, South Korea*

Sang Woong Moon − *Department of Ophthalmology, College of Medicine, Kyung Hee University, Seoul 02447, South Korea*

Jeongyoon Song − *Department of Surgery, College of Medicine, Kyung Hee University, Seoul 02447, South Korea*

Complete contact information is available at: https://pubs.acs.org/10.1021/acsami.9b19421

Author Contributions

S.K., T.G.K. and S.H.L. contributed equally to this work. S.C., J.S.Y., and J.H.S. designed the experiments. T.G.K., J.H.S., S.W.M., and J.S. approved the IRB and collected the human tears. S.H.L. performed material synthesis and structural characterization. W.K. and A.B. performed Raman measurements and analyzed the data. S.K., W.K., and S.C. contributed with the parts of simulation and calculation. S.K., T.G.K., S.H.L, and S.C. cowrote the paper. S.W.M., J.S., J.H.S., J.S.Y., and S.C. contributed to the discussions and comments on the paper.

Notes

The authors declare no competing financial interest.

■ ACKNOWLEDGMENTS

This work was supported by the National Research Foundation of Korea (2019R1A2C2089239, 2017R1C1B1006736, 2018R1A6A1A03025708, 2018R1C1B6008568, and 2018M3A9E8078812).

■ REFERENCES

(1) Siegel, R. L.; Miller, K. D.; Jemal, A. *Ca-Cancer J. Clin.* **2019**, *69*, 7−34.

(2) Chu, K. C.; Tarone, R. E.; Kessler, L. G.; Ries, L. A. G.; Hankey, B. F.; Miller, B. A.; Edwards, B. K. *J. Natl. Cancer Inst.* **1996**, *88*, 1571−1579.

(3) Hellquist, B. N.; Czene, K.; Hjälm, A.; Nyström, L.; Jonsson, H. *Cancer* **2015**, *121*, 251−258.

(4) Askhar, L.; Zaki, Y. *Saudi Med. J.* **2017**, *38*, 768−771.

(5) Mittal, S.; Kaur, H.; Gautam, N.; Mantha, A. K. *Biosens. Bioelectron.* **2017**, *88*, 217−231.

(6) Li, Y. *Open Biomarkers J.* **2010**, *3*, 26−29.

(7) Zhou, L.; Zhao, S. Z.; Koh, S. K.; Chen, L.; Vaz, C.; Tanavde, V.; Li, X. R.; Beuerman, R. W. *J. Proteomics* **2012**, *75*, 3877−3885.

(8) Choi, S.; Moon, S. W.; Shin, J.-H.; Park, H.-K.; Jin, K.-H. *Anal. Chem.* **2014**, *86*, 11093−11099.

(9) Evans, V.; Vockler, C.; Friedlander, M.; Walsh, B.; Willcox, M. D. *Clin. Exp. Ophthalmol.* **2001**, *29*, 161−163.

(10) Lebrecht, A.; Boehm, D.; Schmidt, M.; Koelbl, H.; Grus, F. H. *Cancer Genomics Proteomics* **2009**, *6*, 75−84.

(11) Böhm, D.; Keller, K.; Pieter, J.; Boehm, N.; Wolters, D.; Siggelkow, W.; Lebrecht, A.; Schmidt, M.; Kölbl, H.; Pfeiffer, N.; Grus, F.-H. *Oncol. Rep.* **2012**, *28*, 429−438.

(12) Cong, S.; Wang, Z.; Gong, W.; Chen, Z.; Lu, W.; Lombardi, J. R.; Zhao, Z. *Nat. Commun.* **2019**, *10*, 678.

(13) Lee, H. K.; Lee, Y. H.; Phang, I. Y.; Wei, J.; Miao, Y. E.; Liu, T.; Ling, X. Y. *Angew. Chem. Int. Ed.* **2014**, *53*, 5054−5058.

(14) Liu, G.-q.; Yu, M.-d.; Liu, Z.-q.; Liu, X.-s.; Huang, S.; Pan, P.-p.; Wang, Y.; Liu, M.-l.; Gu, G. *Nanotechnology* **2015**, *26*, 185702.

(15) Liu, G.; Liu, Y.; Tang, L.; Liu, X.; Fu, G.; Liu, Z. *Nanophotonics* **2019**, *8*, 1095−1107.

(16) Le Ru, E. C.; Etchegoin, P. G. *MRS Bull.* **2013**, *38*, 631−640.

(17) Kim, W.; Lee, S. H.; Ahn, Y. J.; Lee, S. H.; Ryu, J.; Choi, S. K.; Choi, S. *Biosens. Bioelectron.* **2018**, *111*, 59−65.

(18) Kim, W.; Lee, S. H.; Kim, J. H.; Ahn, Y. J.; Kim, Y.-H.; Yu, J. S.; Choi, S. *ACS Nano* **2018**, *12*, 7100−7108.

(19) Kim, W.; Lee, S. H.; Kim, S. H.; Lee, J.-C.; Moon, S. W.; Yu, J. S.; Choi, S. *ACS Appl. Mater. Interfaces* **2017**, *9*, 5891−5899.

(20) Kim, W.-S.; Shin, J.-H.; Park, H.-K.; Choi, S. *Sens. Actuators, B* **2016**, *222*, 1112−1118.
(21) Wen, X.; Li, G.; Zhang, J.; Zhang, Q.; Peng, B.; Wong, L. M.; Wang, S.; Xiong, Q. *Nanoscale* **2014**, *6*, 132−139.
(22) Ye, W.; Chen, Y.; Zhou, F.; Wang, C.; Li, Y. *J. Mater. Chem.* **2012**, *22*, 18327−18334.
(23) Alvarez-Puebla, R. A.; Dos Santos, D. S., Jr; Aroca, R. F. *Analyst* **2004**, *129*, 1251−1256.
(24) Zhu, W.; Wu, Y.; Yan, C.; Wang, C.; Zhang, M.; Wu, Z. *Materials* **2013**, *6*, 5625−5638.
(25) Hadobás, K.; Kirsch, S.; Carl, A.; Acet, M.; Wassermann, E. F. *Nanotechnology* **2000**, *11*, 161−164.
(26) Yu, M.; Huang, Z.; Liu, Z.; Chen, J.; Liu, Y.; Tang, L.; Liu, G. *Sens. Actuators, B* **2018**, *262*, 845−851.
(27) McCreery, R. L. *Raman Spectroscopy for Chemical Analysis*; John Wiley & Sons, Inc.: Hoboken, NJ, USA, 2000.
(28) Liu, X.; Shao, Y.; Tang, Y.; Yao, K. F. *Sci. Rep.* **2015**, *4*, 5835.
(29) Le Ru, E. C.; Blackie, E.; Meyer, M.; Etchegoin, P. G. *J. Phys. Chem. C* **2007**, *111*, 13794−13803.
(30) Gautam, R.; Vanga, S.; Ariese, F.; Umapathy, S. *EPJ Instrum. Tech.* **2015**, *2*, 8.
(31) Talari, A. C. S.; Movasaghi, Z.; Rehman, S.; Rehman, I. U. *Appl. Spectrosc. Rev.* **2015**, *50*, 46−111.
(32) Manciu, F. S.; Ciubuc, J. D.; Parra, K.; Manciu, M.; Bennet, K. E.; Valenzuela, P.; Sundin, E. M.; Durrer, W. G.; Reza, L.; Francia, G. *Technol. Canc. Res. Treat.* **2017**, *16*, 461−469.
(33) Surmacki, J.; Brozek-Pluska, B.; Kordek, R.; Abramczyk, H. *Analyst* **2015**, *140*, 2121−2133.
(34) Keller, M. D.; Vargis, E.; de Matos Granja, N.; Wilson, R. H.; Mycek, M.-A.; Kelley, M. C.; Mahadevan-Jansen, A. *J. Biomed. Optic.* **2011**, *16*, 077006.
(35) Leon, S. A.; Shapiro, B.; Sklaroff, D. M.; Yaros, M. J. *Cancer Res.* **1977**, *37*, 646−650.
(36) Silva, J. M.; Dominguez, G.; Garcia, J. M.; Gonzalez, R.; Villanueva, M. J.; Navarro, F.; Provencio, M.; San Martin, S.; España, P.; Bonilla, F. *Cancer Res.* **1999**, *59*, 3251−3256.
(37) Silva, J. M.; Dominguez, G.; Villanueva, M. J.; Gonzalez, R.; Garcia, J. M.; Corbacho, C.; Provencio, M.; España, P.; Bonilla, F. *Br. J. Cancer* **1999**, *80*, 1262−1264.
(38) Schwarzenbach, H.; Pantel, K. *Breast Cancer Res.* **2015**, *17*, 136.
(39) Stroun, M.; Lyautey, J.; Lederrey, C.; Olson-Sand, A.; Anker, P. *Clin. Chim. Acta* **2001**, *313*, 139−142.
(40) Wiggins, T.; Kumar, S.; Markar, S. R.; Antonowicz, S.; Hanna, G. B. *Cancer Epidemiol. Biomark. Prev.* **2015**, *24*, 32−38.
(41) Poschke, I.; Mao, Y.; Kiessling, R.; de Boniface, J. *J. Transl. Med.* **2013**, *11*, 290.
(42) Cascino, A.; Muscaritoli, M.; Cangiano, C.; Conversano, L.; Laviano, A.; Ariemma, S.; Meguid, M. M.; Rossi, F. F. *Anticancer Res.* **1995**, *15*, 507−510.
(43) Fröbe, A.; Čičin-Šain, L.; Jones, G.; Soldič, Ž.; Lukač, J.; Bolanča, A.; Kusič, Z. *Anticancer Res.* **2014**, *34*, 1167−1179.
(44) Mazouni, C.; Arun, B.; André, F.; Ayers, M.; Krishnamurthy, S.; Wang, B.; Hortobagyi, G. N.; Buzdar, A. U.; Pusztai, L. *Br. J. Cancer* **2008**, *99*, 68−71.
(45) da Soares, N. C. P.; Teodoro, A. J.; Lotsch, P. F.; Granjeiro, J. M.; Borojevic, R. *Histol. Histopathol.* **2015**, *30*, 1143−1154.
(46) Leoncini, E.; Nedovic, D.; Panic, N.; Pastorino, R.; Edefonti, V.; Boccia, S. *Cancer Epidemiol. Biomark. Prev.* **2015**, *24*, 1003−1011.
(47) Vieira, A. R.; Abar, L.; Vingeliene, S.; Chan, D. S. M.; Aune, D.; Navarro-Rosenblatt, D.; Stevens, C.; Greenwood, D.; Norat, T. *Ann. Oncol.* **2016**, *27*, 81−96.
(48) Chajès, V.; Romieu, I. *Maturitas* **2014**, *77*, 7−11.

https://dx.doi.org/10.1021/acsami.9b19421
ACS Appl. Mater. Interfaces 2020, 12, 7897−7904